

The Mpemba effect demonstrated on a single trapped ion qubit

Shahaf Aharony Shapira^{†,*}, Yotam Shapira[†], Jovan Markov,
Gianluca Teza, Nitzan Akerman, Oren Raz, and Roei Ozeri
Department of Physics of Complex Systems

Weizmann Institute of Science, Rehovot 7610001, Israel

[†] These authors contributed equally to this work

The Mpemba effect is a counter-intuitive phenomena in which a hot system reaches a cold temperature faster than a colder system, under otherwise identical conditions. Here we propose a quantum analog of the Mpemba effect, on the simplest quantum system, a qubit. Specifically, we show it exhibits an inverse effect, in which a cold qubit reaches a hot temperature faster than a hot qubit. Furthermore, in our system a cold qubit can heat up exponentially faster, manifesting the strong version of the effect. This occurs only for sufficiently coherent systems, making this effect quantum mechanical, i.e. due to interference effects. We experimentally demonstrate our findings on a single $^{88}\text{Sr}^+$ trapped ion qubit.

Physical systems undergoing relaxation can exhibit a wide range of rich and non-trivial phenomena. A prominent example is the Mpemba effect (ME) [1, 2], in which an initially hot system cools down faster than a colder, otherwise identical, system. Some systems manifest a stronger version of this effect [3], in which the hotter systems relaxes exponentially faster. The ME has been experimentally demonstrated in various classical systems, e.g. water [2], Clathrate hydrates [4], magnetic alloys [5], colloids diffusing in a potential [6] and a few others [7–9]. An inverse-ME, in which an initially colder system heats up faster than a warmer system, has been predicted [10, 11] and recently measured [12]. Much theoretical insight was gained on this effect in recent years, using various theoretical methods [13–23] and numerical results [24–27].

Quantum versions of the ME have been recently proposed [28–33], including its extensions in terms of relaxation of entanglement asymmetry in quantum spin-systems [34]. The latter has been recently demonstrated using trapped-ions [35].

Here we propose and experimentally demonstrate the existence of an inverse-ME in the simplest quantum system - a single qubit. We consider a coherently driven qubit that is coupled to a thermal Markovian bath, causing decoherence of the qubit and its eventual relaxation to a non-equilibrium steady state. Our only assumption on the qubit-bath coupling is that the qubit's decoherence rate is monotonically increasing with the bath's temperature. This occurs, e.g., for a black-body photon-emitting bath, such that the emission rate of photons at resonance with the qubit's transition energy increases with temperature. Our analysis shows that a strong inverse-ME can occur, however, only for a sufficiently coherent qubit, making this effect quantum mechanical, i.e. due to interference.

We demonstrate the inverse-ME experimentally by implementing it on the Zeeman qubit, defined on a single trapped $^{88}\text{Sr}^+$ ion. Figure 1 shows our model and the corresponding implementation on the ion's energy levels,

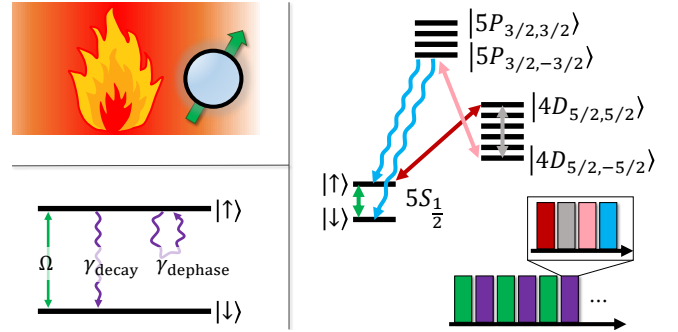


Figure 1. Top left: The modeled quantum system exhibiting an inverse Mpemba-effect. A thermal source of photons (fire) is coupled to coherently driven qubit (blue), causing it to relax to a steady state. Bottom left: The resulting coupling between the qubit's levels, $|\downarrow\rangle$ and $|\uparrow\rangle$, with a coherent drive (green) and decoherence terms causing decay (γ_{decay}) and dephasing (γ_{dephase}). Right: The qubit is mapped to the $5S_{1/2}$ levels of the Zeeman ground state manifold of a trapped $^{88}\text{Sr}^+$ ion. Coherent (green) and incoherent (purple) evolution is generated sequentially (pulse schemes), by using various additional atomic transitions, detailed below.

detailed further below.

The qubit's dynamics is given by the Gorini-Kossakowski-Sudarshan-Lindblad (GKSL) equation, $\partial_t \rho = \mathcal{L}[\rho]$, with \mathcal{L} a Lindblad super-operator, acting on $\rho \in \mathbb{C}^{2 \times 2}$, the density matrix representing a statistical ensemble of a single qubit. Specifically, the operation of the super-operator is given by ($\hbar = 1$),

$$\mathcal{L}[\rho] = -\frac{i\Omega}{2}[\sigma_x, \rho] + \gamma_{\text{decay}}L_{|\uparrow\rangle\langle\downarrow|}[\rho] + \gamma_{\text{dephase}}L_{|\uparrow\rangle\langle\uparrow|}[\rho], \quad (1)$$

with Ω the rate of the coherent driving of the qubit, set by the x -Pauli matrix, σ_x . Open Markovian dynamics are generated by $L_A[\rho] \equiv A\rho A^\dagger - \frac{1}{2}\{A^\dagger A, \rho\}$. We consider decoherence due to decay (dephasing), generated by $|\downarrow\rangle\langle\uparrow|$ ($|\uparrow\rangle\langle\uparrow|$), with rates,

$$\gamma_{\text{decay}} = \alpha\gamma(T), \quad \gamma_{\text{dephase}} = (1 - \alpha)\gamma(T), \quad (2)$$

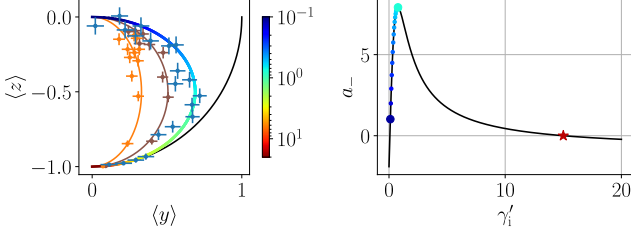


Figure 2. Left: Steady state locus. We measure the qubit's steady-state position (points) on the y - z plane of the Bloch sphere (black line) at different temperatures and compute the corresponding α 's (see the main text). Our data-sets (points) are fitted yielding $\alpha = 0.21 \pm 0.03$ (orange), $\alpha = 0.51 \pm 0.04$ (cyan) and $\alpha = 0.94 \pm 0.07$ (blue), used hereafter. The steady state locus corresponding to the latter is presented in color, showing values of γ_f' (log-scale). Right: Coefficient of the slow-decaying eigenstate, a_- , as a function of γ_i' , for $\gamma_f' = 15$ (red star). The coefficient shows a non-monotonic behaviour, implying the existence of a ME. Furthermore, the curve is shown to vanish at $\gamma_i' = 0.07 \neq \gamma_f'$, proving the existence of a strong-ME. The highlighted circles correspond to the initial states shown in Fig. 3 (with matching colors).

where $0 \leq \alpha \leq 1$, is the relative occurrence of decay. The overall temperature-dependent decoherence rate due to coupling to the bath, $\gamma(T)$, is assumed to be monotonically increasing with T , such that we can characterize the bath by T or γ interchangeably.

The dynamics is conveniently analyzed using the Bloch vector, $\vec{r} = (x, y, z)$, with $\rho = 1/2(1 + \vec{r} \cdot \vec{\sigma})$ (see the Supplemental Material (SM) [36]). Since the system is driven, its fixed points correspond to non-equilibrium steady states that do not obey detailed balance, e.g. the qubit continuously scatters photons. The collection of steady-states, $\vec{r}^{ss}(\gamma)$, form a right-half of an ellipse in the $y - z$ plane, with its center at $(0, 0, -1/2)$ and semiaxes $(r_y, r_z) = (\sqrt{\alpha/2}, 1/2)$, shown in Fig. 2 (left). Each point on this curve, known as the steady state locus, corresponds to a steady state at a given $\gamma' \equiv \gamma/\Omega$, with $\gamma' \rightarrow 0(\infty)$ corresponding to the center (south-pole) of the Bloch sphere.

Consider the relaxation path of an initial condition given by the steady state solution of a cold temperature, $\vec{r}^{ss}(\gamma_i)$, when coupled to a hot bath characterized by γ_f . The solution of Eq. (1) is then given by,

$$\vec{r}(t; \gamma_i, \gamma_f) = \vec{r}^{ss}(\gamma_f) + \sum_{n \in \{+, -, x\}} a_n(\gamma_i, \gamma_f) \vec{v}_n(\gamma_f) e^{\lambda_n(\gamma_f)t}, \quad (3)$$

where $\vec{v}_n(\gamma_f)$ are the relaxation modes of the system, $\lambda_n(\gamma_f)$ their rates, and $a_n(\gamma_i, \gamma_f)$ the corresponding coefficients, determined by the initial and final temperatures [36].

We note that the x -coordinate has a stable fixed point at $x^* = 0$, making the x -direction trivially vanish throughout the system's evolution.

The decay rates in the $y - z$ plane are given by the real

part $\text{Re}[\lambda_{\pm}]$, with

$$\lambda_{\pm} = -\gamma_f' \left(\alpha + 1/2 \pm \sqrt{(\alpha - 1/2)^2 - 1/\gamma_f'^2} \right). \quad (4)$$

The ME can exist only when $\text{Re}[\lambda_{\pm}]$ are distinct, allowing for a slow and fast relaxation modes. This occurs for final temperatures $\gamma_f' > \gamma_b'$, with the bifurcation point $\gamma_b' \equiv |\alpha - 1/2|^{-1}$.

The relaxation at long times is determined by the slowest relaxation mode, λ_- , and its coefficient, a_- , which clearly vanishes for $\gamma_i = \gamma_f$. Fixing γ_f' , one might expect a_- to be monotonic in the range, $0 \leq \gamma_i' \leq \gamma_f'$. However, for an inverse-ME to take place, a cold system must reach the steady state faster than a hotter one, i.e. $|a_-|$ is smaller for a cold system, compared to a hotter system. It is therefore the non-monotonic behavior of a_- as a function of γ_i which enables the existence of the ME [3]. Indeed, the coefficient $a_-(\gamma_i, \gamma_f)$ (full expression in the SM [36]) displays such a behavior, implying the existence of an inverse-ME. An example with $\gamma_f' = 15$ is plotted in Fig. 2 (right).

A strong-ME occurs in the special case in which a_- vanishes at an initial temperature, $\gamma_{i,\text{SME}} \neq \gamma_f$. In that case, the relaxation time is determined by the fast rate, λ_+ , and as a result, it is exponentially faster [3]. In other words, defining the distance to steady state, $d_{ss}^{\gamma_i}(t) \equiv |\vec{r}(t; \gamma_i, \gamma_f) - \vec{r}^{ss}(\gamma_f)|$, then $d_{ss}^{\gamma_i \neq \gamma_{i,\text{SME}}}(t)/d_{ss}^{\gamma_{i,\text{SME}}}(t)$ is asymptotically exponentially increasing in time.

Here, a_- vanishes at $\gamma_{i,\text{SME}} = \gamma_f' \left((\alpha - 1/2) - \sqrt{(\alpha - 1/2)^2 - \gamma_f'^{-2}} \right)$. For example, for $\gamma_f' = 15$, a_- vanishes at $\gamma_{i,\text{SME}}' \approx 0.07$ as seen in Fig. 2 (right). The strong-ME in this system is experimentally optimal to achieve the most pronounced signal (see the SM [36]). Indeed, in our experimental demonstrations we make use of values $\gamma_i \approx \gamma_{i,\text{SME}}$. We mathematically prove the strong-ME can only appear in a heating process, i.e. as an inverse-ME (see the SM [36]).

Since $\gamma_{i,\text{SME}}' > 0$, the required α for a strong-ME is bounded by $\alpha > 1/2 + 1/\gamma_f' \geq 1/2$. When α satisfies this condition, there exists a strong-ME for every final temperature above the bifurcation point, at $\gamma_{i,\text{SME}}'$. Thus, an exponentially faster relaxation occurs only in a coherent enough system, i.e. with a low excess dephasing on top of that induced by the decay channel. Specifically, a classical bit, with no coherence between its two states, cannot exhibit this strong effect.

This model describes, for example, a single trapped $^{88}\text{Sr}^+$ ion qubit in a small-scale quantum computer [37]. Specifically we encode the $|\downarrow\rangle$ ($|\uparrow\rangle$) qubit state on the $5S_{\frac{1}{2}, -\frac{1}{2}}$ ($5S_{\frac{1}{2}, \frac{1}{2}}$) state in the Zeeman ground state manifold, shown in Fig. 1 (right). The two states are coherently coupled with a magnetic field (green), oscillating at the Zeeman splitting frequency in the $5S_{\frac{1}{2}}$

manifold, generating the qubit's Hamiltonian, $H = \Omega\sigma_x$, with Ω the field's Rabi frequency.

As shown in Fig. 1, we combine the coherent and open dynamics in discrete steps, by interlacing small durations of coherent (green pulse) and open Markovian evolution (purple pulse), i.e. by trotterization. Markovian open dynamics are generated by coupling the qubit levels via fast decaying states [38]. Control over α is gained by making use of sequential cascade of pulses and transitions.

Specifically we use a narrow linewidth laser at 674 nm [39] (red) in order to selectively couple the $|\uparrow\rangle$ state to the $|4D_{\frac{5}{2}, \frac{5}{2}}\rangle$ state in the $4D_{\frac{5}{2}}$ metastable manifold. An additional laser at 1033 nm (pink) couples the $4D_{\frac{5}{2}}$ manifold to the short-lived $5P_{\frac{3}{2}}$. Due to selection rules, only the $|5P_{\frac{3}{2}, \frac{3}{2}}\rangle$ state is populated, which quickly decays back to the $|\uparrow\rangle$ state (blue), resulting in full dephasing, i.e. $\alpha = 0$. By using an additional π -pulse in the $4D_{\frac{5}{2}}$ manifold (grey), between the 674 nm and the 1033 nm pulses, we map the $|4D_{\frac{5}{2}, \frac{5}{2}}\rangle$ state to the $|4D_{\frac{5}{2}, -\frac{5}{2}}\rangle$, which will ultimately decay to the $|\downarrow\rangle$ state, yielding $\alpha \approx 1$.

We demonstrate this control experimentally by initializing the system to the $|\uparrow\rangle$ state and letting it relax to a steady state under $n = 100$ repetitions of interlaced dynamics, analogous to a decay time of $7\gamma_f^{-1}$. After this evolution we perform state tomography to determine the location of the steady state on the Bloch sphere. Figure 2 (left) shows the measured steady states for various values of γ' , forming the elliptically shaped steady state locus (blue points), with a fitted value of $\alpha = 0.94 \pm 0.07$ (gradient line).

Intermediate values of α can be formed by replacing the π -pulse in the $4D_{\frac{5}{2}}$ manifold (grey) with, e.g., a $\pi/2$ -pulse or a $\pi/5$ -pulse, yielding a thinner steady state loci, fitted as $\alpha = 0.51 \pm 0.04$ and $\alpha = 0.21 \pm 0.03$, (cyan and orange) respectively.

A canonical experimental protocol for measuring the ME, comprises letting the system relax to the steady state $\vec{r}^{ss}(\gamma'_i)$, then quenching it to a final temperature, γ'_f , while performing tomography of the relaxation dynamics to $\vec{r}^{ss}(\gamma'_f)$. The measurements are then used to obtain the Euclidean-distance on the Bloch sphere from the final steady state, $d_{ss}(t)$. This protocol raises a technical challenge, namely, the relaxation time to an initial cold system, with $\gamma'_i \ll 1$, requires a long evolution duration, which may surpass the system's natural coherence time, leading to an effectively reduced and uncontrolled value of α .

We mitigate this challenge by measuring the ME using two complementary techniques: performing the experimental protocol with large trotter steps, thus reducing the total duration of an experiment, or by effectively preparing the qubit in the initial state,

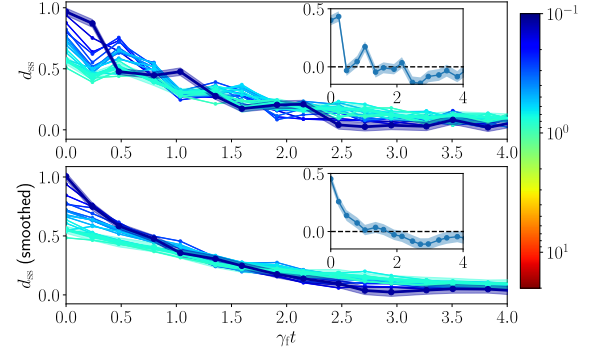


Figure 3. The inverse-ME is demonstrated by relaxing qubits to a steady states at various initial temperatures, γ'_i (color) and tracking their relaxation as a function of time (horizontal) to a final steady state at a fixed temperature, $\gamma'_f = 15 > \gamma'_i$ and $\alpha = 0.94$. We consider the qubit's Euclidean-distance to the final steady state, $d_{ss}(t)$ (vertical). We highlight the distances of an initially cold (thick blue) and hot (thick cyan) systems, d_{ss}^C and d_{ss}^H , respectively, and analyze them further. The insets show $d_{ss}^C - d_{ss}^H$. Error bars (shaded regions) correspond to $\pm 2\sigma$ confidence intervals due to quantum shot-noise. Top: d_{ss} exhibits oscillations, not captured by the model above, which occur due to the relatively large time steps used in the digital evolution. Bottom: Post-processing the same data by polynomial smoothing reproduces the inverse-ME. Specifically, $d_{ss}^C > d_{ss}^H$ at $t = 0$, however their values cross at $t \approx 2\gamma_f^{-1}$, after which $d_{ss}^C < d_{ss}^H$, seen as well in the inset as a negative value, beyond the error bars.

$\vec{r}^{ss}(\gamma'_i)$, thus circumventing the long initial relaxation time.

The results obtained by the former technique, large trotter steps, are shown in Fig. 3. Specifically we evolve the system to $t = 4\gamma_f^{-1}$ in 14 trotter-steps (horizontal) and present $d_{ss}(t)$ (vertical) for various γ'_i 's (color). These steps form a less accurate approximation of the continuous model. Indeed, Fig. 3 (top) exhibits oscillations which are common to non-adiabatic digitized evolution. We highlight an initially cold system, γ_i^C (blue) and an initially hot system, γ_i^H (cyan), which are analyzed in further detail. Specifically the inset shows the distance between these two systems during relaxation, $d_{ss}^C(t) - d_{ss}^H(t)$, which similarly exhibits oscillations.

We compensate for the oscillations by employing simple polynomial-smoothing of the data, shown in Fig. 3 (bottom). This demonstrate an inverse-ME, as the curves of the cold and hot systems cross, with the cold system reaching the steady state before the hot system. Indeed, the inset shows that $d_{ss}^C(0) - d_{ss}^H(0) > 0$, indicating the cold system is initially at a larger distance from steady state. However, during the relaxation we observe a crossing time t_{cross} after which $d_{ss}^C(t) - d_{ss}^H(t) < 0$, beyond $\pm 2\sigma$ error bars due to quantum shot noise.

Next, we directly prepare the qubit at an initial

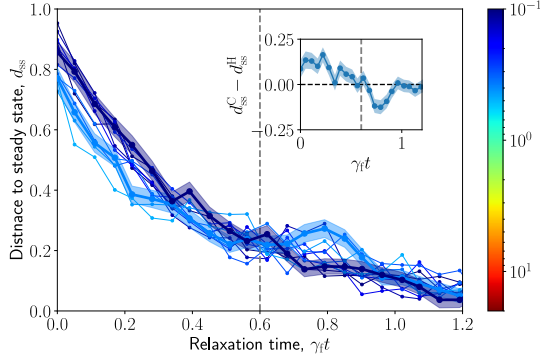


Figure 4. The inverse-ME realized with initial state preperation. The qubit's distance to the final steady state, $d_{ss}(t)$, is shown for qubits initialized at different temperatures (color) and quenched to $\gamma_f' = 100$ and $\alpha = 0.94$. We highlight d_{ss}^C (thick dark blue) and d_{ss}^H (thick light blue), initially cold and hot systems, respectively, and present their $\pm 2\sigma$ confidence intervals (shaded regions). As shown, the hot qubit starts closer to the final steady state. However, at $t_{\text{cross}} \approx 0.6\gamma_f^{-1}$ (vertical grey) the cold system surpasses the hot system and relaxes first, manifesting the inverse Mpemba effect. Inset: $d_{ss}^C(t) - d_{ss}^H(t)$ highlighting the crossing of the two systems, beyond the confidence intervals.

steady state. To do so we write the initial steady state density matrix, ρ_i^{ss} , as a linear combination of two pure-state density matrices. Then, the evolution of ρ_i^{ss} is equivalent to the same linear combination of evolved pure states. Specifically, here the steady states are all of the form, $\rho_i^{\text{ss}} = \frac{1-p}{2} |\theta\rangle\langle\theta| + \frac{1+p}{2} |-\theta\rangle\langle-\theta|$, with θ and p representing the direction and distance of the steady state from the Bloch sphere origin and $|\pm\theta\rangle \equiv \exp[-\frac{i}{2}(\theta \pm \frac{\pi}{2})\sigma_x]|\uparrow\rangle$ (see the SM [36]). An observable stemming from the evolution of ρ_i^{ss} , is recovered by measuring the same observable on the evolution of $|\pm\theta\rangle$, and using a weighted linear combination of the measured observables, with weights $(1 \mp p)/2$.

Figure 4 shows the dynamics of system initialized at steady states with respect to various γ_i' 's, and tracks their evolution as a function of time (horizontal) towards a fixed $\gamma_f' = 100 > \gamma_i'$. Similarly to Fig. 3, we show the distance to the final steady state, d_{ss} , and highlight an initially cold (dark blue) and hot (light blue) systems. As above, $d_{ss}^C(0) > d_{ss}^H(0)$, indicating the cold system is initially at a larger distance from steady state, yet during the relaxation we observe a crossing time t_{cross} after which $d_{ss}^C(t) < d_{ss}^H(t)$, beyond $\pm 2\sigma$ error bars due to quantum shot noise. This is also reflected in the inset which shows $d_{ss}^C - d_{ss}^H$ (vertical) initially positive and at later times negative, beyond the error bars.

In conclusion, we have proposed and experimentally demonstrated the inverse ME on a single qubit. Furthermore, we have proven that a strong, i.e. exponentially faster relaxation, ME exists only for a sufficiently coherent qubit. As our findings pertain the

simplest quantum system, one expects to find the ME in larger quantum systems, such as quantum computers, in which maintaining a low temperature for long times is crucial.

This work was supported by the Israel Science Foundation Quantum Science and Technology (Grant 3457/21). O.R. is supported by the ISF (Grant 232/23). G. T. is supported by the Center for Statistical Mechanics at the Weizmann Institute of Science, the Simons Foundation (grant 662962), the grants HALT and Hydrotronics of the EU Horizon 2020 program and the NSF-BSF (grant 2020765).

* shahaf.aharony@weizmann.ac.il

- [1] E. B. Mpemba and D. G. Osborne, Cool?, *Physics Education* **4**, 172 (1969).
- [2] M. Jeng, The Mpemba effect: When can hot water freeze faster than cold?, *American Journal of Physics* **74**, 514 (2006).
- [3] I. Klich, O. Raz, O. Hirschberg, and M. Vucelja, Mpemba index and anomalous relaxation, *Phys. Rev. X* **9**, 021060 (2019).
- [4] Y.-H. Ahn, H. Kang, D.-Y. Koh, and H. Lee, Experimental verifications of Mpemba-like behaviors of clathrate hydrates, *Korean J. Chem. Eng.* **33**, 1903 (2016).
- [5] P. Chaddah, S. Dash, K. Kumar, and A. Banerjee, Overtaking while approaching equilibrium (2010), [arXiv:1011.3598 \[cond-mat.stat-mech\]](https://arxiv.org/abs/1011.3598).
- [6] A. Kumar and J. Bechhoefer, Exponentially faster cooling in a colloidal system, *Nature* **584**, 64 (2020).
- [7] C. Hu, J. Li, S. Huang, H. Li, C. Luo, J. Chen, S. Jiang, and L. An, Conformation directed mpemba effect on polylactide crystallization, *Crystal Growth & Design* **18**, 5757 (2018), <https://doi.org/10.1021/acs.cgd.8b01250>.
- [8] J. Liu, J. Li, B. Liu, I. W. Hamley, and S. Jiang, Mpemba effect in crystallization of polybutene-1, *Soft Matter* **19**, 3337 (2023).
- [9] M. Chorazewski, M. Wasiak, A. V. Sychev, V. I. Korotkovskii, and E. B. Postnikov, The curious case of 1-ethylpyridinium triflate: Ionic liquid exhibiting the Mpemba effect, *J. Solution Chem.* (2023).
- [10] Z. Lu and O. Raz, Nonequilibrium thermodynamics of the markovian mpemba effect and its inverse, *Proceedings of the National Academy of Sciences* **114**, 5083 (2017).
- [11] A. Lasanta, F. Vega Reyes, A. Prados, and A. Santos, When the hotter cools more quickly: Mpemba effect in granular fluids, *Phys. Rev. Lett.* **119**, 148001 (2017).
- [12] A. Kumar, R. Chérite, and J. Bechhoefer, Anomalous heating in a colloidal system, *Proceedings of the National Academy of Sciences* **119**, e2118484119 (2022).
- [13] M. R. Walker and M. Vucelja, Anomalous thermal relaxation of langevin particles in a piecewise-constant potential, *Journal of Statistical Mechanics: Theory and Experiment* **2021**, 113105 (2021).
- [14] R. Holtzman and O. Raz, Landau theory for the mpemba effect through phase transitions, *Communications Physics* **5**, 280 (2022).

- [15] J. Degünther and U. Seifert, Anomalous relaxation from a non-equilibrium steady state: An isothermal analog of the mpemba effect, *Europhysics Letters* **139**, 41002 (2022).
- [16] D. M. Busiello, D. Gupta, and A. Maritan, Inducing and optimizing markovian mpemba effect with stochastic reset, *New Journal of Physics* **23**, 103012 (2021).
- [17] G. Teza, R. Yaacoby, and O. Raz, Eigenvalue crossing as a phase transition in relaxation dynamics, *Phys. Rev. Lett.* **130**, 207103 (2023).
- [18] F. J. Schwarzendahl and H. Löwen, Anomalous cooling and overcooling of active colloids, *Physical review letters* **129**, 138002 (2022).
- [19] S. Zhang and J.-X. Hou, Theoretical model for the mpemba effect through the canonical first-order phase transition, *Physical Review E* **106**, 034131 (2022).
- [20] G. Teza, R. Yaacoby, and O. Raz, Relaxation shortcuts through boundary coupling, *Physical review letters* **131**, 017101 (2023).
- [21] A. Biswas, V. Prasad, O. Raz, and R. Rajesh, Mpemba effect in driven granular maxwell gases, *Physical Review E* **102**, 012906 (2020).
- [22] A. Santos and A. Prados, Mpemba effect in molecular gases under nonlinear drag, *Physics of Fluids* **32** (2020).
- [23] R. Chétrite, A. Kumar, and J. Bechhoefer, The metastable Mpemba effect corresponds to a non-monotonic temperature dependence of extractable work, *Front. Phys.* **9**, 141 (2021).
- [24] M. Baity-Jesi, E. Calore, A. Cruz, L. A. Fernandez, J. M. Gil-Narvión, A. Gordillo-Guerrero, D. Iñiguez, A. Lasanta, A. Maiorano, E. Marinari, *et al.*, The mpemba effect in spin glasses is a persistent memory effect, *Proceedings of the National Academy of Sciences* **116**, 15350 (2019).
- [25] A. Gal and O. Raz, Precooling strategy allows exponentially faster heating, *Physical review letters* **124**, 060602 (2020).
- [26] A. Gijón, A. Lasanta, and E. Hernández, Paths towards equilibrium in molecular systems: The case of water, *Physical Review E* **100**, 032103 (2019).
- [27] N. Vadakkayil and S. K. Das, Should a hotter paramagnet transform quicker to a ferromagnet? monte carlo simulation results for ising model, *Physical Chemistry Chemical Physics* **23**, 11186 (2021).
- [28] F. Carollo, A. Lasanta, and I. Lesanovsky, Exponentially accelerated approach to stationarity in markovian open quantum systems through the mpemba effect, *Phys. Rev. Lett.* **127**, 060401 (2021).
- [29] S. Kochsiek, F. Carollo, and I. Lesanovsky, Accelerating the approach of dissipative quantum spin systems towards stationarity through global spin rotations, *Phys. Rev. A* **106**, 012207 (2022).
- [30] A. Nava and M. Fabrizio, Lindblad dissipative dynamics in the presence of phase coexistence, *Phys. Rev. B* **100**, 125102 (2019).
- [31] A. K. Chatterjee, S. Takada, and H. Hayakawa, Quantum mpemba effect in a quantum dot with reservoirs, *Phys. Rev. Lett.* **131**, 080402 (2023).
- [32] C. Rylands, K. Klobas, F. Ares, P. Calabrese, S. Murciano, and B. Bertini, Microscopic origin of the quantum mpemba effect in integrable systems, *arXiv preprint arXiv:2310.04419* (2023).
- [33] F. Ivander, N. Anto-Sztrikacs, and D. Segal, Hyperacceleration of quantum thermalization dynamics by bypassing long-lived coherences: An analytical treatment, *Phys. Rev. E* **108**, 014130 (2023).
- [34] S. Murciano, F. Ares, I. Klich, and P. Calabrese, Entanglement asymmetry and quantum mpemba effect in the xy spin chain (2023), *arXiv:2310.07513 [cond-mat.stat-mech]*.
- [35] L. K. Joshi, J. Franke, A. Rath, F. Ares, S. Murciano, F. Kranzl, R. Blatt, P. Zoller, B. Vermersch, P. Calabrese, C. F. Roos, and M. K. Joshi, Observing the quantum mpemba effect in quantum simulations (2024), *arXiv:2401.04270 [quant-ph]*.
- [36] Supplemental material, including additional derivation and technical information.
- [37] T. Manovitz, Y. Shapira, L. Gazit, N. Akerman, and R. Ozeri, Trapped-ion quantum computer with robust entangling gates and quantum coherent feedback, *PRX Quantum* **3**, 010347 (2022).
- [38] E. Ben Av, Y. Shapira, N. Akerman, and R. Ozeri, Direct reconstruction of the quantum-master-equation dynamics of a trapped-ion qubit, *Phys. Rev. A* **101**, 062305 (2020).
- [39] L. Peleg, N. Akerman, T. Manovitz, M. Alon, and R. Ozeri, Phase stability transfer across the optical domain using a commercial optical frequency comb system (2019), *arXiv:1905.05065 [physics.atom-ph]*.

Supplemental Material

1. ANALYTIC SOLUTION OF THE LINDBLAD EQUATION

We provide additional information concerning the solution of the qubit's dynamics. The Lindbladian in the main text can be transformed, using the Kronecker product, into a linear form: $\partial_t \vec{\rho} = \hat{L} \vec{\rho}$, where $\vec{\rho}$ is a column vector and \hat{L} is a 4×4 matrix. For our model, given in Eq. (1) of the main text, we obtain

$$\hat{L}(\Omega, \gamma, \alpha) = \begin{pmatrix} -2\alpha\gamma & -\frac{i\Omega}{2} & \frac{i\Omega}{2} & 0 \\ -\frac{i\Omega}{2} & -\gamma & 0 & \frac{i\Omega}{2} \\ \frac{i\Omega}{2} & 0 & -\gamma & -\frac{i\Omega}{2} \\ 2\alpha\gamma & \frac{i\Omega}{2} & -\frac{i\Omega}{2} & 0 \end{pmatrix}, \quad (5)$$

such that the equation of motion reads,

$$\begin{cases} \dot{\rho}_{11} = -2\alpha\gamma\rho_{11} + \frac{i\Omega}{2}(\rho_{12} - \rho_{21}), \\ \dot{\rho}_{21} = \frac{i\Omega}{2}(\rho_{22} - \rho_{11}) - \gamma\rho_{21}, \\ \dot{\rho}_{12} = \frac{i\Omega}{2}(\rho_{11} - \rho_{22}) - \gamma\rho_{12}, \\ \dot{\rho}_{22} = 2\alpha\gamma\rho_{11} + \frac{i\Omega}{2}(\rho_{21} - \rho_{12}). \end{cases} \quad (6)$$

Since $\rho = \rho^\dagger$ and $\text{Tr}[\rho] = 1$, the state of a single qubit can be equivalently written in the Bloch vector representation:

$$\vec{r} = (\rho_{12} + \rho_{21}, i(\rho_{12} - \rho_{21}), \rho_{11} - \rho_{22}) \equiv (x, y, z). \quad (7)$$

Thus, the set of ordinary differential equations is

$$\begin{cases} \dot{x} = -\gamma x, \\ \dot{y} = -\gamma y - \Omega z, \\ \dot{z} = -2\alpha\gamma(1 + z) + \Omega y. \end{cases} \quad (8)$$

The steady state solution of this system is given by:

$$x^* = 0, \quad y^* = \frac{\Omega/\gamma}{1 + \frac{\Omega^2}{2\alpha\gamma^2}}, \quad z^* = -\frac{1}{1 + \frac{\Omega^2}{2\alpha\gamma^2}}, \quad (9)$$

where the first coordinate, x , is decoupled from the dynamics with a stable fixed point (under the physical assumption $\gamma > 0$). The remaining $2D$ first order differential equation for the $y - z$ -coordinates is given by,

$$\dot{\vec{r}}_2 = \begin{pmatrix} -\gamma & -\Omega \\ \Omega & -2\alpha\gamma \end{pmatrix} \vec{r}_2 + \begin{pmatrix} 0 \\ -2\alpha\gamma \end{pmatrix}, \quad \vec{r}_2 \equiv \begin{pmatrix} y \\ z \end{pmatrix}. \quad (10)$$

Their steady state solution are written in terms of the dimensionless variable $\gamma' \equiv \gamma/\Omega$:

$$y^* = \frac{1}{\gamma' \left(1 + \frac{1}{2\alpha\gamma'^2}\right)} = -\frac{z^*}{\gamma'}, \quad z^* = -\frac{1}{1 + \frac{1}{2\alpha\gamma'^2}} = -\gamma' y^*. \quad (11)$$

These solutions, known as the steady state locus, form the right-half of an ellipse described by

$$\left(\sqrt{\frac{2}{\alpha}} y^*\right)^2 + (2z^* + 1)^2 = 1. \quad (12)$$

The θ and p representation, utilized in the main text for direct state preparation, can be derived by setting, $y^* = p \cos(\theta)$ and $z^* = p \sin(\theta)$, yielding, $p = \frac{2\alpha\gamma'\sqrt{1+\gamma'^2}}{1+2\alpha\gamma'^2}$ and $\theta = -\arctan(\gamma')$.

The homogeneous part of Eq. (10) can be solved by diagonalization. The corresponding eigenvalues are given in Eq. (4) of the main text and are presented in Fig. 5. Since the rates are dictated by their real parts, there exists a bifurcation point, $\gamma'_b \equiv |\alpha - 1/2|^{-1}$. The strong ME exists only at final temperatures larger than the bifurcation point ($\gamma_f > \gamma_b$), i.e. the point at which the degeneracy between eigenvalues breaks and there are distinct fast and

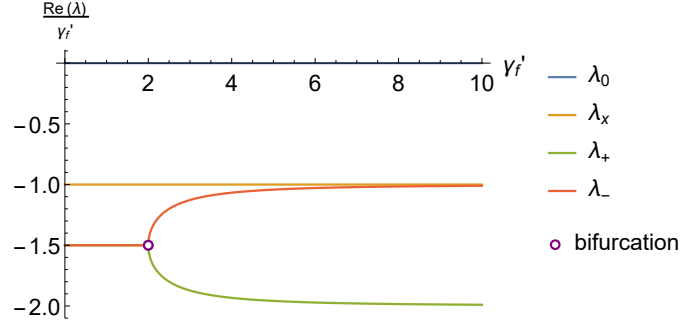


Figure 5. The real part of the system's eigenvalues over final temperature, for $\alpha = 1$. The largest eigenvalue, corresponds to the steady state, zeros. For $H \propto \sigma_x$, the equation for x decouples and the set can be solved analytically. In our case, $\lambda_x = -\gamma_f$. The last couple eigenvalues, λ_{\pm} , correspond to the dynamics in the $y - z$ plane and are therefore interesting. A ME can only occur after the degeneracy is lifted.

slow relaxation modes.

The appropriate (normalized) eigenvectors are given by

$$\vec{v}_{\pm} = \frac{1}{2\alpha - 1} \begin{pmatrix} \frac{1}{\gamma_f' \left(\alpha - 1/2 \pm \sqrt{(\alpha - 1/2)^2 - 1/\gamma_f'^2} \right)} \\ 1 \end{pmatrix}. \quad (13)$$

The coefficients of these modes are given by $a_n(\gamma_i, \gamma_f) \equiv \vec{u}_n(\gamma_f) \cdot \vec{r}^{\text{ss}}(\gamma_i)$, where \vec{u}_n are left eigenvectors, i.e row vectors satisfying the equation,

$$\vec{u}_n \begin{pmatrix} -\gamma & -\Omega \\ \Omega & -2\alpha\gamma \end{pmatrix} = \lambda_n \vec{u}_n. \quad (14)$$

Explicitly, we obtain

$$a_{\pm} = \frac{\alpha \cdot (\alpha - 1/2)}{\sqrt{(\alpha - 1/2)^2 - 1/\gamma_f'^2} (2\alpha + 1/\gamma_f'^2) (2\alpha + 1/\gamma_i'^2)} \left(\frac{\gamma_f'}{\gamma_i'} - 1 \right) \times \left[4\alpha \left(\mp \alpha \pm 1/2 + \sqrt{(\alpha - 1/2)^2 - 1/\gamma_f'^2} \right) - \frac{2}{\gamma_i' \gamma_f'} \left(\mp \alpha \mp 1/2 + \sqrt{(\alpha - 1/2)^2 - 1/\gamma_f'^2} \right) \pm \frac{2}{\gamma_f'^2} \right]. \quad (15)$$

By inserting $\gamma_{i, \text{SME}}$ given in the main text, a_- indeed vanishes.

2. THE ABSENCE OF A STRONG DIRECT-ME

For a strong ME to exist, the coefficient of slow relaxation a_- must vanish. Therefore, in the case of a strong effect the dynamics is along the fast relaxation eigenvector, \vec{v}_+ , only. The fast relaxation eigenvector of a given final temperature γ_f' must therefore intersect the steady state locus in an additional point, corresponding to the ideal initial temperature $\gamma_{i, \text{SME}}'$.

For $\alpha > \frac{1}{2}$, both entries of v_+ are positive (See (13)), such that v_+ points to the up-right direction. On the steady state locus, the temperature is monotonic in z such that states located higher on the locus necessarily correspond to lower temperatures. Moreover, since $\gamma_f' > \gamma_b'$ for a ME to occur, and the crossing of the steady state locus with the bifurcation-line of $\alpha > \frac{1}{2}$ is located in the southern-hemisphere of the locus (See Fig. 6), states located to the right on the locus also correspond to lower temperatures. The implications are that all possible fast vectors point to lower initial temperatures, relative to γ_f' . Accordingly, this system doesn't exhibit a strong, direct, ME.

An explicit illustration of the orientation of \vec{v}_+ , with respect to the steady state locus of $\alpha = 1$, is presented in Fig. 7.

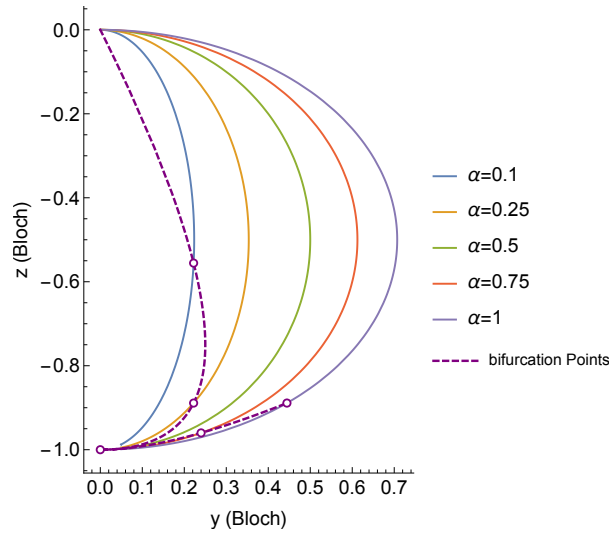


Figure 6. The steady state loci in the $y - z$ plane of the Bloch sphere, as given by Eq. (9), for different values of α , as a function of temperature $\gamma' \in (0, 20]$. The ME exists only at temperatures above γ_b , represented by circles at the crossing with the bifurcation (purple dashed) line. We observe two bifurcation branches, however, only the lower one, crosses loci of $\alpha \geq 1/2$, is valid for a strong ME.

3. THE EXISTENCE OF A STRONG INVERSE-ME

In the main text we prove the existence of a strong inverse-ME by a vanishing of the coefficient of the slow relaxation mode, a_- . As complementary proof to the existence of the strong ME, one simply tracks the evolution of states, near the final steady state. In the long-time limit, fast relaxation modes have already decayed. Assuming a_- crosses zero continuously - it changes signs. Thus, states initialized before and after the zero-crossing will approach the final steady state from opposite directions of \vec{v}_- in the $y - z$ plane. An example is shown in Fig. 8.

An experimental observation of the ME involves comparing the dynamics of a cold and hot initial states, $d_{SS}^C(t)$ and $d_{SS}^H(t)$, respectively. Specifically, the inverse ME is demonstrated by showing that the initially colder system reaches the final steady state faster, although it starts further away. Namely, at the beginning of the experiment $d_{SS}^C(t=0) > d_{SS}^H(t=0)$, whereas after some later time, t_{cross} , the colder system surpasses the hotter such that the distances are reversed, i.e. $d_{SS}^C(t > t_{\text{cross}}) < d_{SS}^H(t > t_{\text{cross}})$.

Measuring $d_{SS}^C(t) < d_{SS}^H(t)$ is inherently challenging, as the two quantities are exponentially decaying. The existence of a strong-ME is helpful due to two reasons: Early onset of the crossing between the cold and hot distances from final steady state, and maximal distance post-crossing. The former allows for short coherence-time of the experimental apparatus and the latter requires less experimental repetitions. Both parameters are optimized at $\gamma_i \sim \gamma_{i,\text{SME}}$. Figure 9 shows this by fixing $\gamma'_{i,H} = 0.77$ and plotting the crossing time (left), as well as the maximal distance to various choices of $\gamma'_{i,C}$ after the two distances cross (right). Clearly, the minimal crossing time, as well as maximal distance between the two decaying signals appear at $\gamma'_i = \gamma'_{i,\text{SME}}$ (vertical gray).

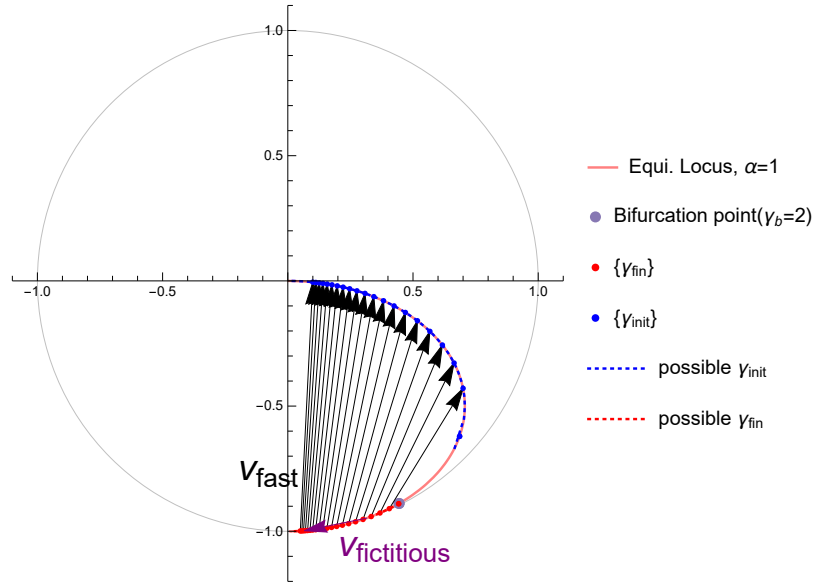


Figure 7. The steady state locus for $\alpha = 1$ (pink line), inside the Bloch sphere (grey line), and three kinds of key points. The first is the bifurcation point, γ'_b (purple dot), which is always located in the southern-hemisphere of the locus. Since the strong ME exists only at final temperatures above this point, the second kind is $\gamma'_f > \gamma'_b$ (red dotted line). We show the fast relaxation vector, v_+ , for various possible final temperatures (black lines). Each of these vectors intersects with the steady state locus at a point corresponds to $\gamma'_{i, SME}$, which is the initial temperature for the strong effect. Blue dotted line: the appropriate possible initial temperatures, for $\gamma_f > \gamma_b$. All possible initial temperatures are smaller than the bifurcation point, i.e. no strong direct effect. In other words, the absence of a vector pointing to higher temperatures, e.g. purple line, refutes the existence of a strong direct effect.

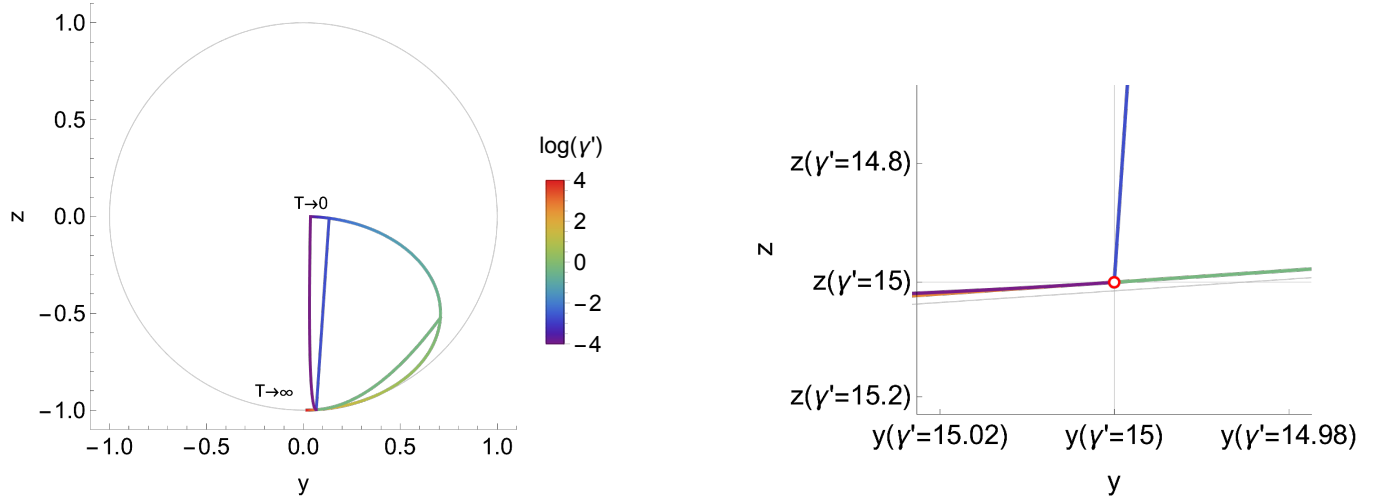


Figure 8. Left: The dynamics of three initial states towards the same final steady-state $\gamma'_f = 15$ (red dot). In order to achieve a strong ME for that final temperature, the corresponding initial temperature is $\gamma'_{SME,i} \approx 0.07$. Since at $\gamma'_{i, cold} \approx 0.07$ (blue line) the coefficient of slow relaxation vanishes, it exhibits an exponentially faster relaxation, compared, for example, to a colder $\gamma'_{i, colder} = 0.02$ (purple line) and hotter $\gamma'_{i, hot} \approx 0.74$ (green line) initial states. Right: The evolution of $\gamma'_{i, cold}$ is along the direction of v_+ only, and a zoom-in on the end of the process reveals how lower and higher initial temperatures approach relaxation from opposite directions, along v_- .

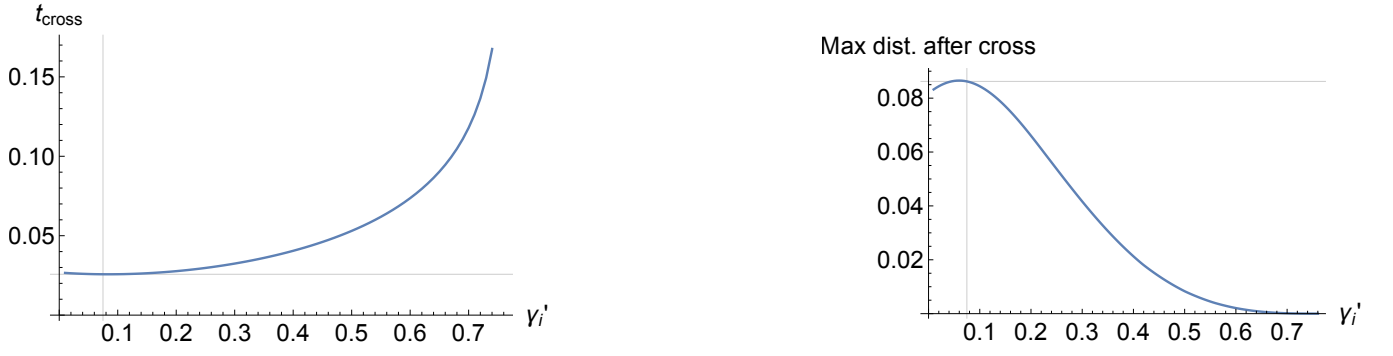


Figure 9. Left: The crossing time of states initialized at γ_i' compared to $\gamma_{i,h}' = 0.77$, while relaxing to $\gamma_f' = 15$. Right: The corresponding maximal distance, post-crossing. The peak indicates the initial state yielding the most pronounced effect, $\gamma_{i,\text{SME}}'$ (grey line), for which the effect is strong.